2005

Absorption and Backscattering in the Beaufort and Chukchi Seas

Jian Wang
Old Dominion University

Glenn F. Cota
Old Dominion University

David A. Ruble
Old Dominion University

Absorption and backscattering in the Beaufort and Chukchi Seas

Jian Wang, Glenn F. Cota, and David A. Ruble

Center for Coastal Physical Oceanography, Department of Ocean, Earth, and Atmospheric Sciences, Old Dominion University, Norfolk, Virginia, USA

[1]   Bio-optical observations were made during August 2000 in the Beaufort and Chukchi Seas. Chlorophyll a concentration (Chl) ranged from 0.068 to 18.5 mg chl m^{-3}. Both total particulate and phytoplankton absorption at 443 nm were closely correlated with chlorophyll concentration. Linear spectral relationships were observed for phytoplankton absorption. The chlorophyll-specific absorption of phytoplankton at 443 nm was nearly constant at 0.013 m^2 (mg chl)$^{-1}$, but particulate absorption due to nonpigmented particulates at 443 nm was highly variable. There was no strong correlation between chlorophyll concentration and absorption by soluble materials or nonpigmented particulates. Absorption, scattering, and attenuation all show strong first-order spectral relationships. Robust relationships between backscattering and chlorophyll and backscattering and remote sensing reflectance were evident. These relationships can be used to construct absorption-based algorithms to retrieve various optical constituents.

Citation: Wang, J., G. F. Cota, and D. A. Ruble (2005), Absorption and backscattering in the Beaufort and Chukchi Seas, *J. Geophys. Res.*, *110*, C04014, doi:10.1029/2002JC001653.

1.   Introduction

[2]   The Arctic Ocean and its adjacent seas play important roles in global biogeochemical cycles and in regulating global oceanic circulation. It has been suggested that increased atmospheric temperatures, resulting from anthropogenic release of greenhouse gases, would have profound effects on the Arctic. Despite its pivotal role, the Arctic Ocean is difficult to sample because of long periods of ice cover and darkness in the region. Advances in new technologies, including satellite remote sensing, have provided alternative ways to synoptically monitor and study the large-scale physical and biological processes occurring within the Arctic Ocean. However, application of satellite remote sensing in ocean studies relies on accurate bio-optical information for this region. Previous studies have suggested that bio-optical properties in polar waters are markedly different from lower-latitude ecosystems [*Mitchell and Holm-Hansen*, 1991; *Mitchell*, 1992; *Sathyendranath et al.*, 2001] with highly packaged cells and lower chlorophyll-specific absorption. Therefore accurate chlorophyll retrieval, which is the primary goal of satellite remote sensing of ocean color, for these regions relies on region-specific algorithms and bio-optical models [*Carder et al.*, 1999; *Reynolds et al.*, 2001] involving inherent optical properties (IOPs), apparent optical properties (AOPs) and chlorophyll.

[3]   The IOPs depend only upon the medium and are independent of the ambient light field [*Mobley*, 1994], but are fundamental to understand and predict light propagation within a water body. Spectral light absorption and back-scattering are two IOPs of primary importance, because they are directly related to remote sensing measurements of ocean color. Several recent studies have examined the spectral relationships for IOPs. These relationships can be used to predict other IOPs from select measured IOPs at a single wavelength. *Barnard et al.* [1998] discovered linear relationships in the IOPs spectra based on the measurements made at 488 nm from a "global" data set. Their data set included 1914 vertical profiles from open ocean to estuarine environments, spanning a broad range of environmental conditions. They pointed out that more specific regional models should be developed for more accurate prediction of IOPs on regional scales. *Gould et al.* [1999] described linear spectral relationships for the scattering coefficients for various environments, and developed a simplified model to estimate the scattering coefficient at any wavelength from a known scattering value at a single wavelength. In this study, we examine spectral relationships for absorption, scattering and beam attenuation based on bio-optical data collected in the Beaufort and Chukchi Seas during August 2000.

[4]   The remote sensing reflectance R_{rs} (see Table 1 for symbols, definitions and units), defined as the ratio of water-leaving radiance L_w to downwelling irradiance E_d, is an apparent optical property (AOP) that depends on both the medium and the geometric structure of the ambient light field. Apparent optical properties such as R_{rs} and L_w are very important to remote sensing application, for example, the current Ocean Color four-band (OC4) algorithms [*O'Reilly et al.*, 2000] for NASA Sea-viewing Wide Field-of-View Sensor (SeaWiFS) use the maximum band ratio of R_{rs} for the band combinations of 443/555, 490/555, or 510/555. In this paper, the variability of absorption and backscattering were investigated to develop region-specific

Table 1. Notation and Units

Symbol	Definition	Unit
L_w	water-leaving radiance	W m^{-2} sr^{-1}
L_{wn}	normalized water-leaving radiance	sr^{-1}
L_u	in-water upwelling radiance	W m^{-2} sr^{-1}
E_d	downwelling irradiance	W m^{-2}
E_u	upwelling irradiance	W m^{-2}
E_s	above-water incident irradiance	W m^{-2}
R_{rs}	remote sensing reflectance(= L_w/E_d)	sr^{-1}
Chl	chlorophyll concentration	mg m^{-3}
a_t	total absorption coefficient	m^{-1}
a_w	water absorption coefficient	m^{-1}
a_p	total particulate absorption coefficient(= $a_a + a_n$)	m^{-1}
a_n	nonpigmented particulates absorption coefficient	m^{-1}
a_a	phytoplankton absorption coefficient	m^{-1}
a_s	soluble materials absorption coefficient	m^{-1}
a_{t-w}	total absorption coefficient minus water(= $a_p + a_s$)	m^{-1}
a_{cdm}	nonpigmented plus soluble materials absorption coefficient(= $a_n + a_s$)	m^{-1}
a_a^*	chlorophyll-specific absorption coefficient for phytoplankton	m^2 mg^{-1}
b_p	particulate scattering coefficient	m^{-1}
b_b	total backscattering coefficient	m^{-1}
b_{bw}	water backscattering coefficient	m^{-1}
b_{bp}	particulate backscattering coefficient	m^{-1}
c	beam attenuation coefficient	m^{-1}
λ	wavelength	nm
γ	parameter describing backscattering spectral dependency	
S	spectral decay constant for soluble materials absorption	nm^{-1}
F	proportionality factor between R_{rs} and b_b/a	
Q	ratio of upwelling irradiance to upwelling radiance	sr

models to link R_{rs} with chlorophyll and inherent optical properties. Spectral dependencies of absorption, scattering, and attenuation were studied to gain more insight into fundamental relationships of individual IOPs. Our primary objective was to develop relationships for IOPs as needed for bio-optical modeling and chlorophyll retrieval algorithms for the Arctic Ocean.

2. Methods

[5] Bio-optical observations were made on board USCGC *Polar Star* from 7 to 31 August 2000 in the Beaufort and Chukchi Seas. This cruise to the Arctic Ocean in 2000 is hereafter referred to as "Arc00." Figure 1 shows the station map of the cruise. There were 29 optical stations spanning the area from about 168° to 144°W and 70° to 75°N, covering parts of the shelf, slope, and basin regions of the Beaufort and Chukchi Seas. Most of the stations were on the shelves, which were largely ice-free or <50% ice-covered by August. Discrete water samples were collected for chlorophyll and spectral absorption analyses. Passive optical profiles determined spectral reflectance (Satlantic profiler with surface reference). An active instrument package was deployed to measure spectral absorption, beam attenuation (WET Labs ac-9), and backscattering (HOBI Labs HydroScat-6) within the water column. Two ac-9 instruments measured total (without water) and soluble (<0.2 μm) absorption. Owing to adverse weather conditions, optical instruments were not deployed at all stations. Nevertheless, our data set from Arc00 represents the most comprehensive field measurements of optical properties in the Beaufort and Chukchi Seas to date. Note that the data were only from summer and application to other Arctic regions should be cautious.

2.1. Discrete Water Samples

[6] Discrete water samples for chlorophyll and absorption were collected with Niskin bottles at six light depths corresponding to 100%, 50%, 30%, 15%, 5% and 1% of surface irradiance according to the Secchi Disk at most stations. Triplicate samples were collected at the surface (100% light level). Water samples were filtered onto 25 mm Whatman glass fiber filters (GF/F). The filters were extracted in 90% acetone at −20°C in the dark for ∼24 hours, and chlorophyll *a* concentrations (Chl) of the extract were measured with a Turner Design fluorometer using standard fluorometric methodology [*Strickland and Parsons*, 1972].

[7] Spectral absorption was determined on particulate and filter-passing or soluble fractions with discrete samples. Total particulate absorption coefficients were measured according to the filter pad technique of *Mitchell* [1990] after concentration on Whatman GF/F filters with a nominal pore size of 0.7 μm. All samples were analyzed within one hour of filtration. The absorption coefficients of total particulate matter, $a_p(\lambda)$, were measured on a Shimadzu 2401 dual beam scanning spectrometer from 280 nm to 850 nm at 1 nm spectral resolution using a moist GF/F filter as a blank. Absorption spectra were normalized to the mean absorption coefficient from 750 nm to 850 nm. Absorption coefficients of nonpigmented particulates $a_n(\lambda)$ were determined after cold methanol extraction [*Kishino et al.*, 1985]. The phytoplankton or algal absorption coefficients, $a_a(\lambda)$, were obtained by subtracting $a_n(\lambda)$ from $a_p(\lambda)$. The absorption coefficients of phytoplankton $a_a(\lambda)$ were then normalized to chlorophyll concentration to obtain chlorophyll-specific absorption coefficients $a_a^*(\lambda)$. There were a total of 157 absorption spectra in Arc00.

[8] Filtrate from GF/F filter was collected and filtered through 0.2 μm Nucleopore membrane for analysis of
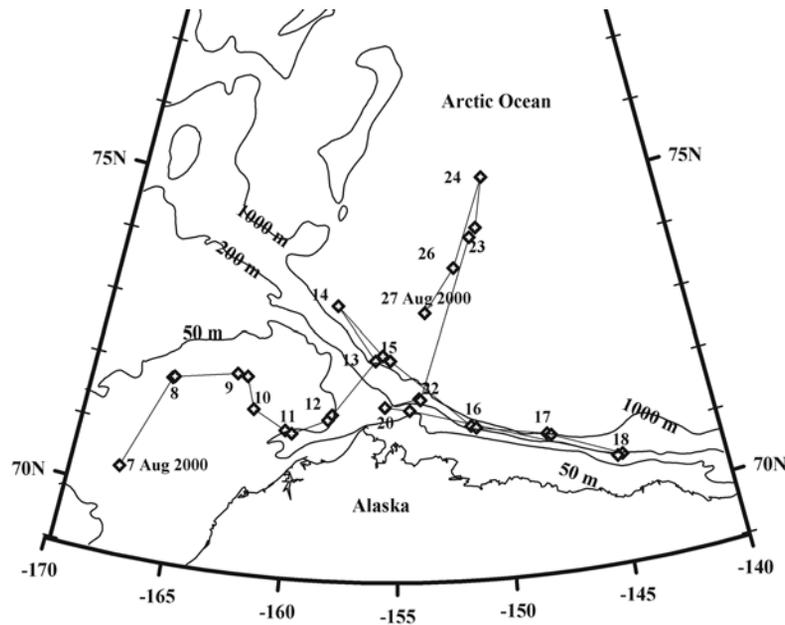
Figure 1. Station locations for the Arctic 2000 cruise in the Beaufort and Chukchi Seas. There were a total of 29 optical stations, and dates in August are shown.

absorption by soluble substances [*Bricaud et al.*, 1981]. A deionized water blank was employed in a 10 cm quartz cuvette. The measured optical densities (ODs) were fitted to a power function ($Y = a + bX^c$), and baseline adjustment was made to the spectra by normalizing the OD values to OD(750 nm). The fitted ODs were converted to absorption coefficients of soluble materials $a_s(\lambda)$. The total absorption coefficient minus water a_{t-w} was considered as the sum of the particulate and soluble absorption coefficients. In our spectrophotometric techniques, materials of size between 0.2 μm and 0.7 μm were ignored. This may include nonattached bacterial and some colloidal materials. Therefore their contributions to total absorption are missing in discrete analyses. Tests from measuring absorption by filtrate directly through 0.7 μm showed the error was relatively small.

2.2. Continuous Profile Observations

2.2.1. Active Optical Measurements

[9] Vertical profiles of absorption and beam attenuation coefficients were measured in situ by an ac-9 meter (WET Labs, Inc.) at nine wavelengths: 412, 440, 488, 510, 555, 630, 650, 676, and 715 nm. A 0.2 μm pore-size cartridge filter was placed at the inlet of the absorption meter of a second ac-9 meter for measuring absorption by soluble materials. Temperature and salinity corrections were applied to absorption and beam attenuation coefficients as described by *Pegau et al.* [1997], and absorption coefficients were further corrected for scattering by subtraction of absorption at 715 nm (ac-9 protocol, WET Labs, Inc.). For Arc00, ac-9 data were binned and had a spatial resolution of 0.5 m, and there were 18 stations with matched ac-9 measurements and discrete sampling.

[10] The ac-9 meters measure total absorption coefficient minus water a_{t-w}, and beam attenuation coefficient c. The scattering coefficient $b(\lambda)$ was calculated by subtracting

the absorption coefficient from the beam attenuation coefficient:

$$b(\lambda) = c(\lambda) - a_{t-w}(\lambda). \qquad (1)$$

Here particulate scattering coefficient b_p is considered equivalent to total scattering coefficient b because molecular scattering by water and soluble materials are small, and normally are negligible compared with that of particulate matter.

[11] There have been few in situ measurements of backscattering coefficients in the Arctic. During Arc00, the backscattering coefficient b_b was measured with a HydroScat-6 backscattering meter (HOBI Labs) at six wavelengths: 443, 488, 510, 555, 676, and 852 nm in the Beaufort and Chukchi Seas. Data from the ac-9 and HydroScat-6 were integrated and acquired with a Modular Ocean Data And Power System (MODAPS, WET Labs).

2.2.2. Passive Optical Measurements

[12] Measurements of downwelling spectral irradiance $E_d(\lambda)$ and upwelling radiance $L_u(\lambda)$ were made with a Satlantic free-fall profiling spectral radiometer and a surface reference at 13 channels: 400, 412, 443, 490, 510, 520, 532, 555, 565, 620, 665, 683, and 700 nm. The instrument includes tilt and roll sensors, a pressure sensor, and a conductivity-temperature sensor. Optical casts were normally made to the depth of 70–100 m, and profiler tilt <5° was considered acceptable. All radiometric sensors were deployed more than 10 m away from the ship to minimize the effects of ship shadow.

[13] Optical data acquisition and analyses were done as described by *Cota et al.* [2003], and were in accordance with then current SeaWiFS protocols [*Mueller and Austin*, 1995]. After correction for attenuation, reflection and refraction, radiance profiles were extrapolated to and through the air-water interface to estimate water-leaving radiance
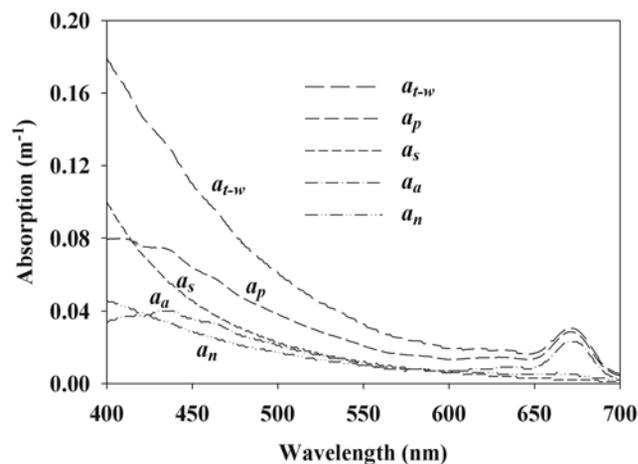
Figure 2. Mean spectra of total absorption minus water a_{t-w}, total particulate absorption a_p, phytoplankton absorption a_a, nonpigmented particulate absorption a_n, and soluble absorption a_s ($n = 157$ spectra).

$L_u(\lambda, 0^+)$. Normalized water-leaving radiance $L_{wn}(\lambda)$ were obtained by normalizing $L_u(\lambda, 0^+)$ to incident solar radiation at the top of the atmosphere. Remote sensing reflectance $R_{rs}(\lambda)$ was computed as the ratio of $L_u(\lambda, 0^+)$ to incident irradiance $E_s(\lambda, 0^+)$ just above the surface. A regional bio-optical algorithm for chlorophyll retrieval [*Wang and Cota*, 2003] was established by regression of ratios of remote sensing reflectance from two or more bands against surface chlorophyll concentrations [*O'Reilly et al.*, 1998, 2000].

3. Results and Discussion

3.1. Absorption

3.1.1. Mean Absorption Spectra

[14] In oceanic waters [*Morel and Prieur*, 1977], the total absorption a_t, is the sum of absorption by water a_w, total particulates a_p, and soluble materials a_s:

$$a_t = a_w + a_p + a_s. \tag{2}$$

Particulate absorption a_p can be further partitioned into algal or phytoplankton absorption a_a and absorption by non-pigmented particulates a_n:

$$a_p = a_a + a_n. \tag{3}$$

[15] Our data set from Arc00 includes 157 individual absorption spectra measured in the euphotic zone of the Beaufort and Chukchi Seas. The mean spectra of absorption by total particulates, phytoplankton, nonpigmented particulates, and soluble materials as well as total absorption coefficient minus water are shown in Figure 2. The effects of chlorophyll absorption on the particulate absorption spectrum are evident from the peaks around 440 and 675 nm (see Figure 2). The mean $a_a(440)$ for the 157 spectra is 0.0397 m^{-1} with a standard deviation of 0.0517, while $a_a(675)$ has a mean value of 0.0233 ± 0.0372 m^{-1}. The mean values for a_p at 440 and 675 nm are 0.0725 ± 0.0707 m^{-1} and 0.0288 ± 0.0411 m^{-1}, respectively. Absorp-

tion by nonpigmented particulates in the blue partially masks the chlorophyll absorption peak around 440 nm in total particulate absorption spectrum. Absorption by soluble materials decreases exponentially with increasing wavelength (Figure 2).

[16] The mean ratio of absorption by phytoplankton to total particulates at 443 nm is 0.51 ± 0.19, which suggests phytoplankton contributes to about half of particulate absorption around the blue peak. *Bricaud et al.* [1998] found that absorption by nonpigmented particulates was a relatively constant portion of total particulate absorption around $25-30\%$ throughout the chlorophyll concentration range from 0.02 to 25 mg m^{-3}. While their data set ($n = 1166$) included much larger and diverse observations from various areas of the world ocean, our data from Arc00 ($n = 157$) showed even larger variability. Absorption by nonpigmented particulates accounts for $10-90\%$ of total particulate absorption at 443 nm for chlorophyll concentrations less than 0.3 mg m^{-3}, which implies that nonpigmented particulates are often more abundant but highly variable in low-biomass waters (Figure 3a). The contribution of absorption by nonpigmented particulates to total particulate absorption is about $20-40\%$ for chlorophyll concentrations higher than 5 mg m^{-3}. Consistent with the results of *Cleveland* [1995] for subpolar region, the proportion of total particulate absorption due to nonpigmented particulates does not exhibit a clear trend with chlorophyll con-
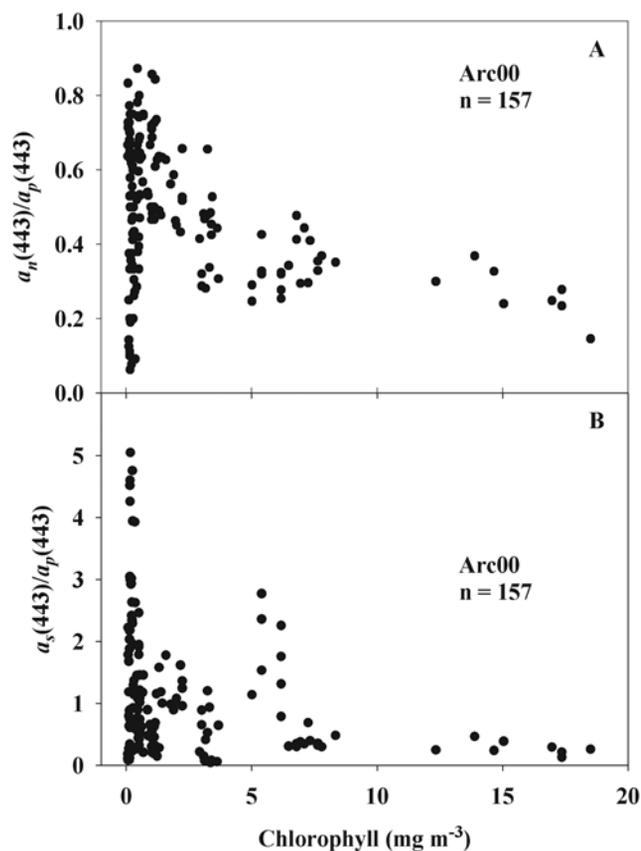

Figure 3. Ratios of absorption by (a) nonpigmented particulates and (b) soluble materials to total particulates at 443 nm versus chlorophyll concentration.
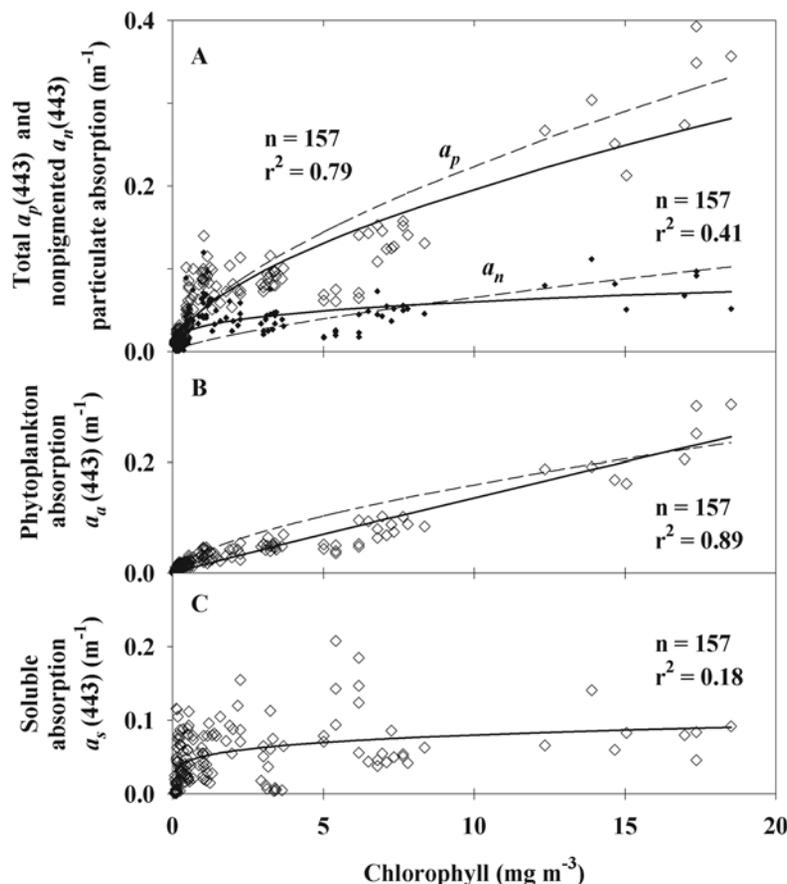
Figure 4. Power functions for (a) total and nonpigmented particulates, (b) phytoplankton, and (c) soluble absorption at 443 nm versus chlorophyll concentration. Filled diamonds refer to nonpigmented particulates. Dashed lines are the relationships of *Bricaud et al.* [1998].

centration for Arc00, but is higher for lower biomass overall (Figure 3a). Similarly, no simple trend was observed for the ratio of soluble absorption to particulate absorption as a function of chlorophyll concentration (Figure 3b). The ratio of soluble absorption to total particulate absorption at 443 nm had an average value of 1.16 ± 1.08. The standard deviation is comparable to the mean ratio in magnitude, showing soluble materials were extremely variable, especially for low chlorophyll concentrations where soluble absorption can be as high as five times of particulate absorption. *Pegau* [2002] reported that soluble materials increase total absorption from 350 to 700 nm by over 30% in the Arctic surface waters. Therefore absorption by soluble materials is important in determining the total absorption in the Arctic waters.

3.1.2. Relationships Between Absorption and Chlorophyll

[17] A power function [*Bricaud et al.*, 1995, 1998] has been suggested to describe the nonlinearity between absorption coefficients and chlorophyll concentrations:

$$a(\lambda) = A(\lambda)[\text{chl}]^{B(\lambda)}, \qquad (4)$$

where A and B are two wavelength-dependent constants. The chlorophyll concentration measured in Arc00 ranged from 0.066 to 18.5 mg m^{-3}, spanning three orders of

magnitude. Nonlinear fits of absorption coefficients at 443 nm of total particulates, nonpigmented particulates, phytoplankton, and soluble materials versus chlorophyll concentration to the power function provided highly significant description of the data:

$$a_p(443) = 0.0511[\text{chl}]^{0.585}, \quad r^2 = 0.79, \quad n = 157, \qquad (5)$$

$$a_a(443) = 0.0151[\text{chl}]^{0.957}, \quad r^2 = 0.89, \quad n = 157, \qquad (6)$$

$$a_n(443) = 0.0306[\text{chl}]^{0.296}, \quad r^2 = 0.41, \quad n = 157, \qquad (7)$$

$$a_s(443) = 0.0509[\text{chl}]^{0.197}, \quad r^2 = 0.18, \quad n = 157, \qquad (8)$$

where r^2 is the coefficient of determination and n is the sample size.

[18] The relationships between absorption coefficients and chlorophyll concentration are illustrated in Figure 4. In this nonlinear model, chlorophyll explains about 80% and 90% of the variability of particulate and phytoplankton absorption, as indicated by r^2 values. The root-mean-square (RMS) errors for these two fits are 0.002 and 0.001 m^{-1},

respectively. *Cota et al.* [2003] previously reported r^2 of 0.80 and 0.70 for absorption by total particulates and phytoplankton for Labrador Sea, and corresponding r^2 of 0.89 and 0.93 for Resolute Bay (G. F. Cota, unpublished data, 1998). *Bricaud et al.* [1998] observed determination coefficients r^2 of 0.90 and 0.91 for particulate and phytoplankton absorption, respectively, with a much larger data set (n = 1166). Their relationships would overestimate particulate and phytoplankton absorption across the observed biomass range of Arc00 (Figures 4a and 4b). The relatively high coefficients of determination for all these regions suggest that the relationships between absorption by total particulates or phytoplankton and chlorophyll are fairly strong in the high northern latitude regions. Chlorophyll is a significant variable to predict absorption by total particulates and phytoplankton, which is important for building chlorophyll-dependent semianalytical models [e.g., *Reynolds et al.*, 2001]. Note that the relationships are only valid within the chlorophyll range over which they were developed, and may not be applicable to other areas or the same area at different times.

[19] About 40% of the variability of the absorption by nonpigmented particulates at 443 nm is explained by this power function with RMS error of 0.002 m^{-1}, which is similar to that observed in Labrador Sea, where about 50% of the variability is accounted for by this model [*Cota et al.*, 2003]. The relationship between absorption by soluble materials and chlorophyll concentration (Figure 4c) only explains 18% of the variability (RMS error of 0.003 m^{-1}). Similar relationships [*DeGrandpre et al.*, 1996; *Nelson et al.*, 1998] suggest soluble materials often do not covary closely with chlorophyll. The composition and quantities of soluble materials in the water column are controlled by many processes, including grazing, sedimentation, photolysis, and bacterial degradation. Furthermore, shelf waters of the Beaufort and Chukchi Seas are influenced by river discharges and ice melting. The annual discharge to the Arctic Ocean has increased by 7% from 1936 to 1999 [*Peterson et al.*, 2002]. The Beaufort Sea receives a total annual discharge of 3.3×10^{11} m^3 yr^{-1} from the Mackenzie River, the fifth highest in the Arctic and the total discharge into the Chukchi Sea is 0.7×10^{11} m^3 yr^{-1} [*Gardeev et al.*, 1996]. Hence it is not surprising that most of the variability of soluble materials cannot be explained by chlorophyll alone, since CDOM is accumulated over growth season and it is unlikely correlated to instantaneous chlorophyll. It is rather controlled by combined effects of many biological, chemical and physical processes. Since the absorption by soluble materials has to be taken into account for interpreting ocean color signatures, the lack of covariance between soluble materials and chlorophyll often complicates accurate chlorophyll retrievals from satellite remote sensing.

[20] In equation (6), the exponent (0.957) is close to 1. In fact, strong linearity was observed between absorption by phytoplankton at 443 nm and chlorophyll concentration (r^2 = 0.91, p < 0.0001), and the linear regression slope of 0.013 m^2 (mg chl)$^{-1}$ was equivalent to the chlorophyll-specific phytoplankton absorption coefficient at 443 nm $a_a^*(443)$. The chlorophyll-specific absorption coefficients of phytoplankton $a_a^*(\lambda)$ describe the in vivo absorption capacity of living algal cells. Phytoplankton cells can be less efficient at harvesting light because their pigments are packaged. The

diminution of the pigment absorption in algal cells is known as pigment packaging [see *Kirk*, 1994]. Examining the red absorption band of chlorophyll *a* near 676 nm, where the influence of accessory pigments is minimal, provides a measure of the pigment packaging effects. The commonly accepted values of $a_a^*(676)$ for unpackaged pigments have the range of 0.023–0.029 m^2 (mg chl)$^{-1}$ [*Johnsen et al.*, 1994; *Moisan and Mitchell*, 1999]. The $a_a^*(676)$ for Arc00 averaged 0.014 ± 0.006 m^2 (mg chl)$^{-1}$, which suggests significant pigment packaging effects in the Beaufort and Chukchi Seas. Pigment packaging can be very significant at high latitudes as phytoplankton cells acclimate themselves to the low-light and nutrient-rich environment. *Cota* [unpublished data] found highly packaged red peak values of 0.006 ± 0.002 m^2 (mg chl)$^{-1}$ for large diatoms near Resolute Bay and 0.010 ± 0.002 m^2 (mg chl)$^{-1}$ for the Labrador Sea [*Cota et al.*, 2003]. Natural variability of a_a^* are normally associated with phytoplankton composition (species, cell size, and pigment composition), or photoacclimation within the local population. Results of pigment analysis using High Performance Liquid Chromatography (HPLC) and size fractionated chlorophyll from spring and summer cruises to the Beaufort and Chukchi Seas in 2002 help better understand the phytoplankton community structure. There appears to be a seasonal succession of phytoplankton in this region (V. Hill et al., Seasonal succession of phytoplankton in the Chukchi and Beaufort Seas, submitted to *Deep-Sea Research*, 2004). Diatoms with cell size larger than 5 μm dominated on the shelf with retreating ice and higher nutrient conditions in spring. In summer, when nutrients were depleted in ice-free waters, smaller prasinophytes and chlorophytes dominated near surface, but diatoms were still abundant at depths of 1–15% of surface irradiance level. The dominance of smaller cells with lower packaging effects in summer corroborates the observation of higher chlorophyll-specific absorption in the Beaufort and Chukchi Seas than some other Arctic regions.

3.1.3. Comparison of Spectrophotometer Analyses and ac-9 Meter Measurements

[21] The combination of spectral absorption obtained from spectrophotometric analyses and by ac-9 measurements can provide both high spectral resolution (1 nm) and spatial resolution (0.5 m). The absorption coefficients obtained from in situ measurements by ac-9 meters and laboratory measurements using discrete water samples were compared to investigate the agreement between the two methods. Simultaneous measurements of absorption coefficients by both methods were taken at 18 stations during Arc00. The average values of the total absorption coefficient minus water a_{t-w} at the surface are presented in Figure 5a. *Pegau et al.* [1995] compared spectral absorption coefficients measured by six different techniques, including laboratory measurements using water samples and in situ measurements. They reported the overall agreement within 40% at 456 nm and 25% at 532 nm. Our results showed that the relative difference between absorption coefficients measured by a spectrophotometer and by ac-9 meters did not exceed 33% at 412, 440, 488, and 510 nm, but was larger than 60% for 555, 630, 650, and 676 nm, which can be attributed to the smaller relative magnitude of absorption coefficients at longer wavelength. Root-mean-square (rms) error between the two measurements was 0.017 m^{-1}.
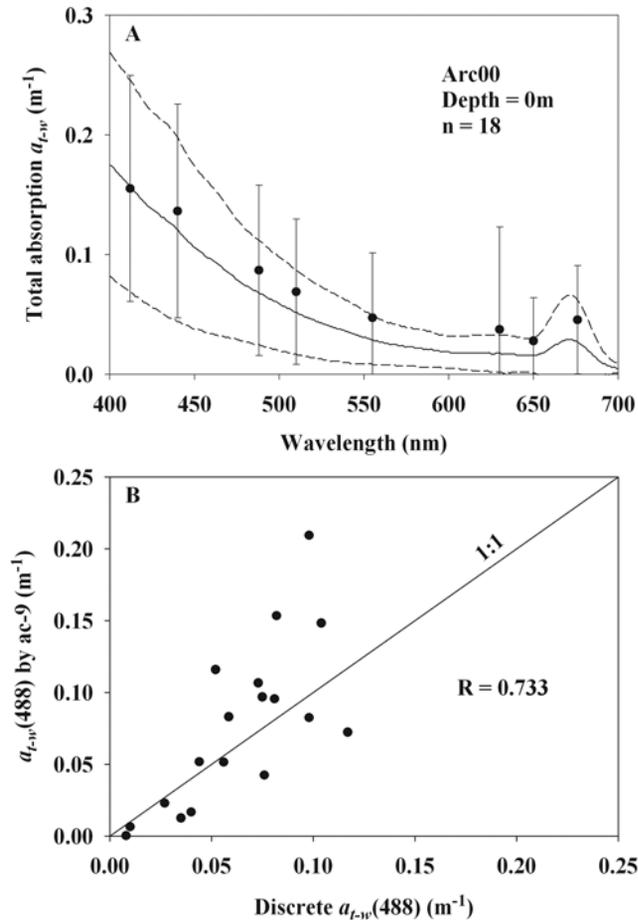
Figure 5. Comparison of (a) total absorption coefficient minus water a_{t-w} at the surface measured by spectrophotometric analyses and by ac-9 meters and (b) correlation for $a_{t-w}(488)$ by the two methods. Mean spectrum (solid line) $\pm$ one standard deviation (dashed line) are shown for spectrophotometric analyses. Measurements by ac-9 at eight wavelengths are shown as dots, and standard deviations are shown as error bars.

[22] In most cases a_{t-w} measured by ac-9 meters agreed well with a_{t-w} obtained from spectrophotometric analyses (see Figure 5a). A possible reason for slightly higher a_{t-w} by ac-9 might be that in our spectrophotometric techniques, contribution to total absorption by materials of size between 0.2 μm and 0.7 μm were not included. To further compare a_{t-w} measured by the discrete (spectrophotometer) and continuous methods (ac-9), correlation of a_{t-w} at 488 nm measured by the two methods are plotted in Figure 5b. The correlation coefficient for $a_{t-w}(488)$ is 0.733. Correlation coefficients for a_{t-w} at eight of ac-9's bands are listed in Table 2. They are higher than 0.70 for all cases showing a_{t-w} measured by the discrete and continuous methods are closely correlated. Comparisons of these two methods at different depths (data not shown) also showed that absorption coefficients measured by ac-9 meters were generally in good agreement with those derived from spectrophotometric analyses. This is promising because simultaneously observations with a spectrophotometer and ac-9 meters can provide both high spectral and high spatial resolutions,

Table 2. Linear Correlation Coefficients Between Total Absorption Minus Water a_{t-w} at the Surface Measured Spectrophotometrically Versus ac-9 Observations at Eight Wavelengths

Wavelength, nm	Correlation Coefficient (R)
412	0.810
440	0.816
488	0.733
510	0.776
555	0.719
630	0.805
650	0.730
676	0.765

and yield much more detailed information about the structure of underwater light fields.

3.2. Backscattering

3.2.1. Relationships Between Backscattering and Chlorophyll

[23] The total backscattering coefficient b_b can be partitioned into backscattering of pure seawater, b_{bw}, and backscattering of particles, b_{bp}:

$$b_b = b_{bw} + b_{bp}. \tag{9}$$

Using a reference wavelength λ_0, the total backscattering coefficient can be formulated as

$$b_b(\lambda) = \left[b_{bw}(\lambda_0) + b_{bp}(\lambda_0) \right] \left(\frac{\lambda_0}{\lambda} \right)^{\gamma}, \tag{10}$$

where γ is a parameter describing the spectral dependency of backscattering, and the reference wavelength is usually chosen to be 555 nm [*Reynolds et al.*, 2001].
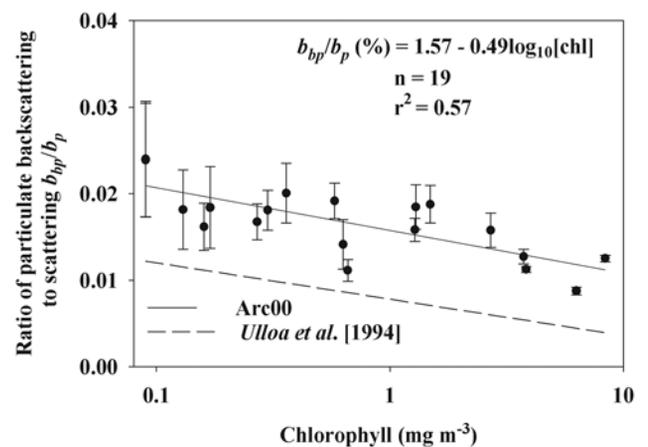

Figure 6. Ratio of particulate backscattering coefficient to total particulate scattering coefficient as a function of chlorophyll concentration. Mean ratio is calculated by averaging ratios at five wavelengths (443, 488, 510, 555, and 676 nm) at each station ($n = 19$). Standard deviations are shown as error bars. Relationship for Arc00 (solid line) is compared with *Ulloa et al.*'s [1994] relationship (dashed line).
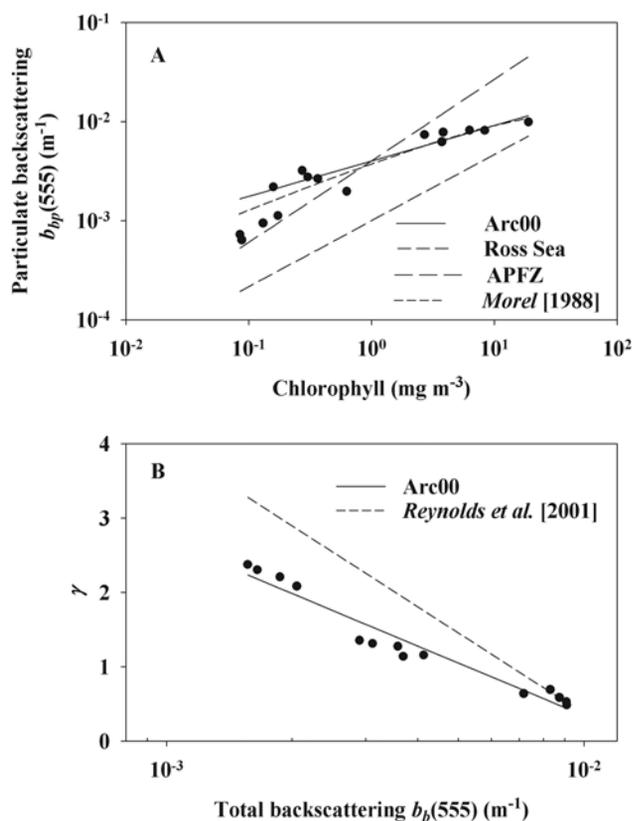
Figure 7. (a) Relationships between backscattering coefficients of particles at 555 nm and chlorophyll concentrations for Arc00, Ross Sea, and APFZ. The relationship predicted by *Morel* [1988] is shown for comparison. (b) Parameter describing backscattering spectral dependency γ as a function of backscattering coefficients at 555 nm for Arc00 (solid line) is compared with *Reynolds et al.*'s [2001] model (dashed line).

[24] In case 1 waters phytoplankton and heterotrophic bacteria account for most of the scattering, while backscattering is mostly due to very small (<1 μm) and abundant nonpigmented particles [*Morel and Ahn*, 1991; *Stramski and Kiefer*, 1991]. *Ulloa et al.* [1994] pointed out that the particulate backscattering to scattering ratio (b_{bp}/b_p) is sensitive to the presence of submicrometer particles and strongly dependent on the shape of particle-size distribution. The particulate backscattering to scattering ratio is a function of particle composition and influenced by both chlorophyll-containing and nonpigmented particles. *Twardowski et al.* [2001] suggested the ratio is related to the refractive index of the samples. Their results showed that the relationship between b_{bp}/b_p and chlorophyll is stronger for high chlorophyll concentration, and becomes more dependent on nonpigmented particles for low chlorophyll concentration. For Arc00, the backscattering to scattering ratios at 443, 488, 510, 555, and 676 nm were calculated using surface values (0∼10 m) from 19 optical stations. Linear regression of mean particulate backscattering to scattering ratio versus logarithm of chlorophyll concentration (Figure 6) gives the following results:

$$b_{bp}/b_p(\%) = 1.57 - 0.49 \log_{10}[\text{chl}], \quad (11)$$

with the r^2 of 0.57 ($p < 0.001$) and RMS error of 0.0006. This approach was based on the assumption that b_{bp}/b_p is wavelength independent, which is in accordance with the theoretical results of *Ulloa et al.* [1994]. The relationship between backscattering to scattering ratio and chlorophyll turns out crucial for selecting the phase function with correct backscattering fraction in HYDROLIGHT simulations of remote sensing reflectance [*Wang and Cota*, 2003]. The regression slope (−0.49) is not significantly different from the slope (−0.42) suggested by *Ulloa et al.* [1994] ($p > 0.05$, F test), but our intercept is significantly higher ($p < 0.0001$, F test). The relatively higher backscattering ratios in our data set suggest larger amounts of nonpigmented particles were present in the environment, since small particles have been reported to significantly contribute to the backscattering ratio [*Risović*, 2003]. Concentrations of nonpigmented particles were presumably high at some Arc00 stations further east past Barrow Canyon (Figure 1) that were influenced by river runoff (e.g., Mackenzie, Colville, etc.). The larger standard deviation of backscattering to scattering ratios for lower chlorophyll concentration (Figure 6) implies higher spectral variability of backscattering to scattering ratios. This observation that backscattering by nonpigmented particles is spectrally more variable for low chlorophyll concentration is consistent with the high variability of particle concentrations at the low-biomass range (Figure 3a). The effect becomes less prominent with increasing chlorophyll concentration because nonpigmented particles concentrations are less variable.

[25] Backscattering coefficients of particulates at 555 nm covary strongly with chlorophyll concentrations (Figure 7a):

$$b_{bp}(555) = 0.004[\text{chl}]^{0.357}, \quad r^2 = 0.91, \quad n = 15. \quad (12)$$

Previously reported relationships between $b_{bp}(555)$ and chlorophyll concentration are also presented in Figure 7a. Our results are consistent with the model of *Morel* [1988]. Across the range of observed biomass, backscattering in the Beaufort and Chukchi Seas is significantly higher than in the Ross Sea. *Reynolds et al.* [2001] suggested that larger cell size or less abundant nonpigmented particulates in the Ross Sea led to the lowered backscattering. Compared with the Antarctic Polar Front Zone (APFZ), backscattering for low-biomass (<1.0 mg chl m^{-3}) waters in the Arctic Ocean is higher, while at higher biomass (>1.0 mg chl m^{-3}) backscattering for Arc00 is lower, as illustrated in Figure 7a. The difference may be caused by more abundant nonpigmented particulates at low biomass in arctic waters (Figure 3a). However, phytoplankton photoadaptation can cause changes in Chl/scattering ratio without changes in biomass. Nutrients, temperature, mixed layer depth (MLZ) can all contribute to the observed variability.

[26] The index of backscattering spectral dependency γ [*Reynolds et al.*, 2001] was strongly correlated with backscattering at 555 nm (Figure 7b):

$$\gamma = -2.348 \log_{10}(b_b(555)) - 4.353, \quad (13)$$

with a determination coefficient of 0.95 ($p < 0.00001$). Together with the above formulation and the relationships
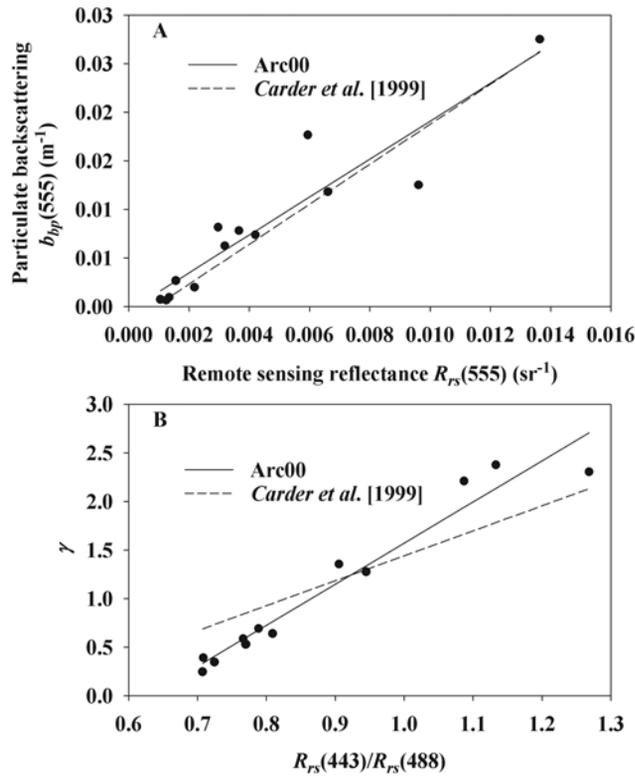
Figure 8. (a) Relationships between backscattering coefficients of particles at 555 nm and remote sensing reflectance at 555 nm, and (b) index of backscattering spectral dependency γ versus ratios of reflectance at 443 nm to 488 nm. Relationships predicted by *Carder et al.* [1999] are illustrated for comparison (dashed lines).

between $b_{bp}(555)$ and chlorophyll, total backscattering can be modeled based upon chlorophyll concentration and $b_{bp}(555)$, both of which can be obtained from field measurements. This approach provides the important backscattering component for constructing bio-optical models relating R_{rs} to chlorophyll and inherent optical properties (IOPs).
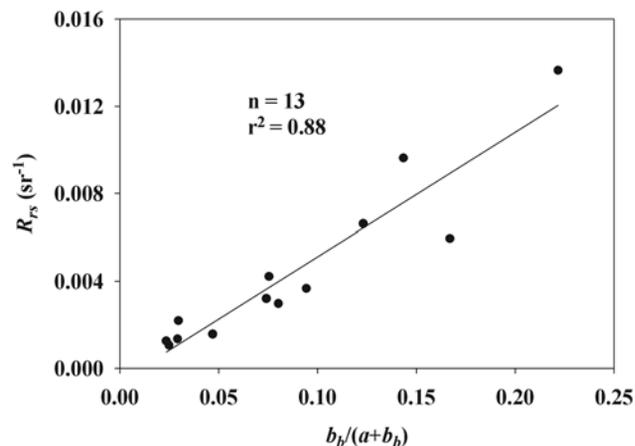

Figure 9. Relationships between remote sensing reflectance and the ratio of backscattering to the sum of absorption and backscattering for 555 nm.

Table 3. Linear Regression Coefficients for Remote Sensing Reflectance R_{rs} Versus the Ratio of Backscattering to the Sum of Backscattering and Absorption $b_b/(b_b + a)$[a]

λ, nm	Slope	Intercept	r^2	$f(\lambda)/Q(\lambda)$
443	0.048	0.0004	0.44	0.089
488	0.067	−0.0017	0.74	0.124
510	0.064	−0.0009	0.83	0.119
555	0.057	−0.0006	0.88	0.106
665	0.053	−0.0001	0.89	0.098

[a]The value of f/Q was calculated by dividing the regression slope by 0.54.

3.2.2. Relationships Between Backscattering and Remote Sensing Reflectance

[27] *Carder et al.* [1999] developed an inverse model for predicting chlorophyll and absorption by phytoplankton and soluble materials from remote sensing reflectance. The relationships between IOPs and R_{rs} are critical to construct such a model. Figure 8a demonstrates that relationship between particulate backscattering coefficients at 555 nm and R_{rs} in Beaufort and Chukchi Seas is very close to that of *Carder et al.* [1999]. The two relationships are not significantly different from each other ($p > 0.05$, F test). The spectral dependency γ also correlates with the ratio of reflectance at 443 nm to 488 nm (Figure 8b), but has a slope different from that of *Carder et al.* [1999] ($p < 0.05$, F test). Note that *Carder*'s [1999] model was developed for particulate backscattering, while in our relationship the parameter γ has a slightly different definition, describing the spectral dependency of total backscattering including backscattering by water. Specific parameterizations for different regions are required to accurately retrieve bio-optical constituents using the model of *Carder et al.* [1999].

[28] The remote-sensing reflectance R_{rs}, is linked to absorption and backscattering through the following formulation [*Lee et al.*, 1994]:

$$R_{rs}(\lambda) = \frac{ft^2}{Q(\lambda)n^2}\left(\frac{b_b(\lambda)}{a(\lambda) + b_b(\lambda)}\right), \quad (14)$$

where f is an empirical factor and is a function of the solar zenith angle [*Kirk*, 1984; *Morel and Gentili*, 1991], t is the transmittance of the air-sea interface, $Q(\lambda)$ is the ratio of upwelling irradiance to radiance $E_u(\lambda)/L_u(\lambda)$, and n is the real part of the refraction index of seawater. Here t^2/n^2 is found to be about 0.54, and relatively independent of wavelength [*Austin*, 1974]. Although individually $f(\lambda)$ and $Q(\lambda)$ may show high variability, the ratio of $f(\lambda)/Q(\lambda)$ is less variable, and can be assumed to be constant [*Gordon et al.*, 1988; *Morel and Gentili*, 1993]. Linear regression of measured R_{rs} versus the ratio of backscattering to the sum of backscattering and absorption, $b_b/(b_b + a)$, at five wavelengths (Table 3) shows that values of f/Q are all within the range of 0.09 to 0.12. The values of f/Q are consistent with those empirically determined by *Reynolds et al.* [2001] and derived from Monte Carlo simulations [*Morel and Gentili*, 1993]. Figure 9 illustrates the linear relationships between R_{rs} and $b_b/(b_b + a)$ at 555 nm for Arc00, with f/Q value of 0.106 (Table 3) and a determination coefficient of 0.88 and RMS error of 0.0003 sr^{-1}.
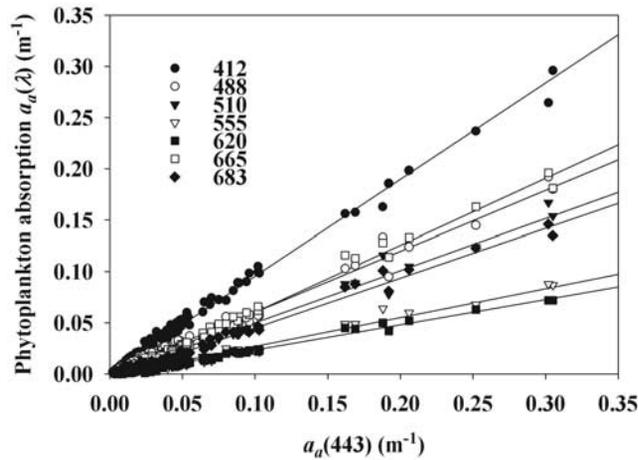
Figure 10. Spectral relationships between phytoplankton absorption at seven wavelengths and phytoplankton absorption at 443 nm. The linear regression fits are shown as lines.

Table 4. Results of Linear Regression of Phytoplankton Absorption at Seven Wavelengths Versus $a_a(443 \text{ nm})$

λ, nm	Slope	Intercept	r^2
412	0.94	0.014	0.99
488	0.59	0.001	0.99
510	0.51	−0.001	0.98
555	0.28	−0.001	0.97
620	0.25	−0.001	0.99
665	0.65	−0.005	0.99
683	0.49	−0.004	0.98

tion coefficients are listed in Tables 5, 6, and 7, respectively. The linear dependencies of these inherent optical properties are pretty strong at almost all wavelengths examined. The regional relationships found in the Arctic corroborate the global relationships [*Barnard et al.*, 1998]. The linear spectral relationships of these IOPs make it possible to predict absorption, scattering, or attenuation from a single wavelength. This is of great importance in satellite remote sensing since bio-optical information is usually limited in most cases. It is crucial that more detailed models be
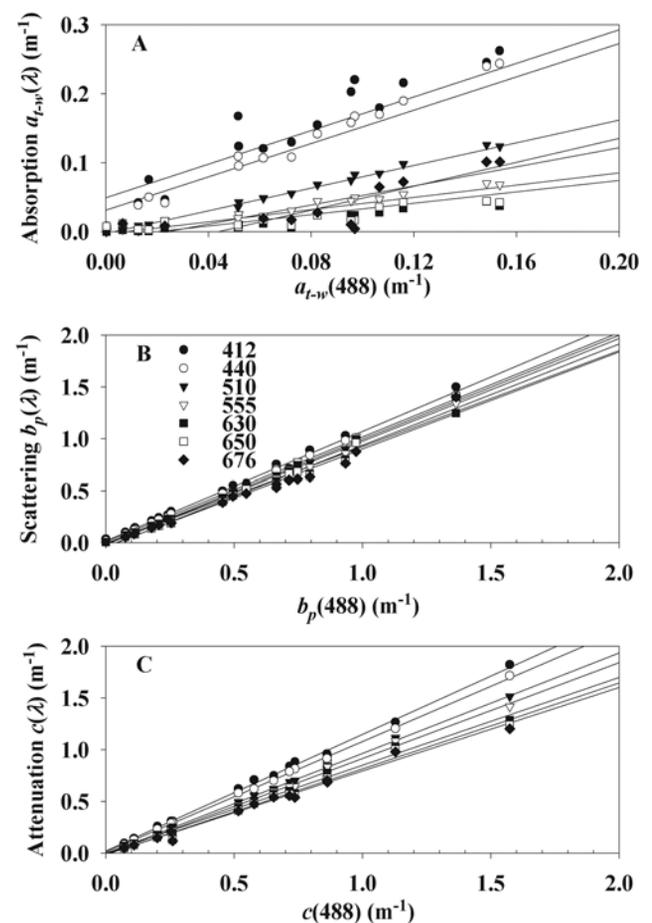
Closure between R_{rs} and IOPs is achieved for all five spectral bands included in our measurements, lending credence to the accuracy of individual measurements. The closure between remote sensing reflectance and inherent optical properties is important for empirical formulations linking R_{rs} to IOPs and accurate modeling of R_{rs} or IOPs.

3.3. Spectral Dependencies of Inherent Optical Properties

[29] Figure 10 shows the strong linear spectral dependencies of phytoplankton absorption observed in the Beaufort and Chukchi Seas. A reference wavelength of 443 nm was chosen because it is a SeaWiFS channel, and around the phytoplankton absorption peak in the blue. The slopes and intercepts for spectral dependencies of phytoplankton absorption are summarized in Table 4, and coefficients of determination r^2 exceed 0.97 for all cases. This relationship is not surprising given that phytoplankton absorption strongly covary with biomass. Combining the spectral dependencies with chlorophyll-specific absorption coefficients for phytoplankton and other constituents, the absorption components of bio-optical models can be parameterized to chlorophyll and absorption at a single wavelength (e.g., 443 nm).

[30] The total absorption coefficients minus water a_{t-w}, scattering coefficients b_p, and beam attenuation coefficients c also exhibited similar linear spectral dependencies (Figures 11a, 11b, and 11c). The spectral dependencies of these IOPs at 488 nm were determined using data from the ac-9 measurements in accordance with *Barnard et al.* [1998]. The spectral dependency of each IOP can be expressed as

$$y(\lambda) = mx(488 \text{ nm}) + b, \quad (15)$$

where m is the slope and b is the intercept. The slopes, intercepts, and coefficients of determination r^2 for absorption coefficients, scattering coefficients, and beam attenua-

Figure 11. Total absorption coefficient minus water a_{t-w} at seven wavelengths versus (a) a_{t-w} at 488 nm, (b) the same relationships for scattering coefficient b_p, (c) and beam attenuation coefficient c. The linear regression fits at each wavelength are shown as lines.

Table 5. Results of Linear Regression of Total Absorption Without Water $a_{t\text{-}w}$ at Seven Wavelengths Versus $a_{t\text{-}w}$ (488 nm)

λ, nm	Slope	Intercept	r^2
412	1.216	0.050	0.843
440	1.208	0.032	0.930
510	0.820	−0.002	0.929
555	0.692	−0.016	0.802
630	0.868	−0.038	0.520
650	0.413	−0.008	0.667
676	0.444	−0.003	0.471

Table 7. Results of Linear Regression of Beam Attenuation c at Seven Wavelengths Versus c (488 nm)

λ, nm	Slope	Intercept	r^2
412	1.127	0.022	0.997
440	1.067	0.013	0.999
510	0.971	−0.005	0.999
555	0.927	−0.010	0.997
630	0.848	0.002	0.992
650	0.831	−0.014	0.990
676	0.807	−0.011	0.988

developed and tuned with IOPs on regional scales for this purpose given the wide range of variability.

4. Conclusions

[31] Bio-optical properties of Arctic waters have been found to be fundamentally different from low-latitude waters [*Mitchell*, 1992; *Cota et al.*, 2003]. Phytoplankton absorption and total particulate absorption at 443 nm both covary closely with chlorophyll concentration across the observed dynamic range of 0.068 to 18.5 mg chl m^{-3}, which suggests that their underlying controlling mechanisms are dominated by the anabolic processes of phytoplankton. The nonpigmented portion of particulate absorption is most variable for low biomass (Chl < 0.3 mg chl m^{-3}). Particulate absorption due to nonpigmented particles increases as chlorophyll concentration decreases. River input to shelf waters and ice melting in summer contribute to the addition of soluble materials. No strong correlation exists between absorption by soluble materials and chlorophyll, which must be related to differences in the controlling catabolic and abiotic processes.

[32] A comparison between spectrophotometric analyses and ac-9 measurements shows that absorption coefficients measured by both methods are generally in good agreement. High spectral and spatial resolutions can be achieved by using both methods simultaneously, which provides more accurate and complete descriptions of the under water light field.

[33] Strong spectral dependencies of phytoplankton absorption are observed. *Barnard et al.* [1998] suggested global relationships of linear spectral dependencies for absorption, scattering, and attenuation, which are supported by our regional data. These first-order relationships can be used to predict absorption, scattering, and attenuation even when information is limited. The spectral dependency of backscattering and relationships between backscattering and chlorophyll are robust as shown by our data. The spectral relationships of IOPs are fundamental, and are very important for developing bio-optical models. Models linking

chlorophyll and IOPs with remote sensing reflectance are more accurate with regionally specific parameterizations. Understanding the variability of each inherent optical property is a prerequisite to develop such models. Parallel efforts include building bio-optical models based on the results presented in this paper, and further evaluating and tuning model performance [*Wang and Cota*, 2003]. These models are of immediate interest in remote sensing applications, and critically important to better understand regional differences in bio-optical properties and remote sensing algorithms.

References

Austin, R. W. (1974), Inherent spectral radiance signatures of the ocean surface, in *Ocean Color Analysis*, pp. 2.1–2.20, Scripps Inst. of Oceanogr., San Diego, Calif.

Barnard, A. H., W. S. Pegau, and J. R. V. Zaneveld (1998), Global relationships of the inherent optical properties of the oceans, *J. Geophys. Res.*, *103*, 24,955–24,968.

Bricaud, A., A. Morel, and L. Prieur (1981), Absorption by dissolved organic matter of the sea (yellow substance) in the UV and visible domains, *Limnol. Oceanogr.*, *26*, 43–53.

Bricaud, A., M. Babin, A. Morel, and H. Claustre (1995), Variability in the chlorophyll-specific absorption coefficients of natural phytoplankton: Analysis and parameterization, *J. Geophys. Res.*, *100*, 13,321–13,332.

Bricaud, A., A. Morel, M. Babin, K. Allali, and H. Claustre (1998), Variations of light absorption by suspended particles with chlorophyll *a* concentration in oceanic (case 1) waters: Analysis and implications for bio-optical models, *J. Geophys. Res.*, *103*, 31,033–31,044.

Carder, K. L., F. R. Chen, Z. P. Lee, S. K. Hawes, and D. Kamykowski (1999), Semianalytic Moderate-Resolution Imaging Spectrometer algorithms for chlorophyll *a* and absorption with bio-optical domains based on nitrate-depletion temperatures, *J. Geophys. Res.*, *104*, 5403–5421.

Cleveland, J. S. (1995), Regional models for phytoplankton absorption as a function of chlorophyll *a* concentration, *J. Geophys. Res.*, *100*, 13,333–13,344.

Cota, G. F., W. G. Harrison, T. Platt, S. Sathyendranath, and V. Stuart (2003), Bio-optical properties of the Labrador Sea, *J. Geophys. Res.*, *108*(C7), 3228, doi:10.1029/2000JC000597.

DeGrandpre, M. D., A. Vodacek, R. K. Nelson, E. J. Bruce, and N. V. Blough (1996), Seasonal seawater optical properties of the U.S. Middle Atlantic Bight, *J. Geophys. Res.*, *101*, 22,727–22,736.

Gardeev, V. V., J. M. Martin, I. S. Sidorov, and M. V. Sidorova (1996), A reassessment of the Eurasian river input of water sediment, major elements, and nutrients to the Arctic Ocean, *Am. J. Sci.*, *296*, 664–691.

Gordon, H. R., O. B. Brown, R. H. Evans, J. W. Brown, R. C. Smith, K. S. Baker, and D. K. Clark (1988), A semi-analytic radiance model of ocean color, *J. Geophys. Res.*, *93*, 10,909–10,924.

Gould, R. W., R. A. Arnone, and P. M. Martinolich (1999), Spectral dependence of the scattering coefficient in case 1 and case 2 waters, *Appl. Opt.*, *38*, 2377–2383.

Johnsen, G., O. Samset, L. Granskog, and E. Sakshaug (1994), In vivo absorption characteristics in 10 classes of bloom-forming phytoplankton: Taxonomic characteristics and responses to photoadaptation by means of discriminant and HPLC analysis, *Mar. Ecol. Prog. Ser.*, *105*, 149–157.

Table 6. Results of Linear Regression of Particulate Scattering Coefficient b_p at Seven Wavelengths Versus b_p (488 nm)

λ, nm	Slope	Intercept	r^2
412	1.051	0.021	0.994
440	1.009	0.008	0.995
510	1.005	−0.009	0.998
555	0.993	−0.016	0.994
630	0.928	−0.004	0.988
650	0.980	−0.042	0.981
676	0.938	−0.035	0.978

Kirk, J. T. O. (1984), Dependence of relationship of between inherent and apparent optical properties of water on solar altitude, *Limnol. Oceanogr.*, *29*, 350–356.

Kirk, J. T. O. (1994), *Light and Photosynthesis in Aquatic Ecosystems*, pp. 254–258, Cambridge Univ. Press, New York.

Kishino, M., M. Takahashi, N. Okami, and S. Ichimura (1985), Estimation of the spectral absorption coefficients of phytoplankton in the sea, *Bull. Mar. Sci.*, *37*, 634–642.

Lee, Z. P., K. L. Carder, S. H. Hawes, R. G. Steward, T. G. Peacock, and C. O. Davis (1994), A model for interpretation of hyperspectral remote-sensing reflectance, *Appl. Opt.*, *33*, 5721–5732.

Mitchell, B. G. (1990), Algorithms for determining the absorption coefficient of aquatic particles using quantitative filter technique (QFT), *Ocean Optics 10, Proc. SPIE Int. Soc. Opt. Eng.*, *1302*, 137–148.

Mitchell, B. G. (1992), Predictive bio-optical relationships for polar oceans and marginal ice zones, *J. Mar. Syst.*, *3*, 91–105.

Mitchell, B. G., and O. Holm-Hansen (1991), Bio-optical properties of Antarctic Peninsula waters: Differentiation from temperate ocean models, *Deep Sea Res.*, *38*, 1009–1028.

Mobley, C. (1994), *Light and Water: Radiative Transfer in Natural Waters*, pp. 60–61, Elsevier, New York.

Moisan, T. A., and B. G. Mitchell (1999), Photophysiological acclimation of *Phaeocystis antarctica* Karsten under light limitation, *Limnol. Oceanogr.*, *44*, 247–258.

Morel, A. (1988), Optical modeling of the upper ocean in relation to its biogenous matter content (case 1 waters), *J. Geophys. Res.*, *93*, 10,749–10,768.

Morel, A., and Y.-H. Ahn (1991), Optics of heterotrophic nanoflagellates and ciliates: A tentative assessment of their scattering role in oceanic waters compared to those of bacteria and algal cells, *J. Mar. Res.*, *49*, 177–202.

Morel, A., and B. Gentili (1991), Diffuse reflectance of oceanic waters: Its dependence on Sun angle as influenced by molecular scattering contribution, *Appl. Opt.*, *30*, 4427–4438.

Morel, A., and B. Gentili (1993), Diffuse reflectance of oceanic waters, II, Bi-directional aspects, *Appl. Opt.*, *32*, 6864–6879.

Morel, A., and L. Prieur (1977), Analysis of variations in ocean color, *Limnol. Oceanogr.*, *22*, 709–722.

Mueller, J. L., and R. W. Austin (1995), Ocean optics protocols for Sea-WiFS validation, revision 1, *NASA Tech. Mem.*, *25*(104566), 67 pp.

Nelson, N. B., D. A. Siegel, and A. F. Michaels (1998), Seasonal dynamics of colored dissolved material in the Sargasso Sea, *Deep Sea Res., Part I*, *45*, 931–957.

O'Reilly, J. E., S. Maritorena, B. G. Mitchell, D. A. Siegel, K. L. Carder, S. A. Garver, M. Kahru, and C. McClain (1998), Ocean color chlorophyll algorithms for SeaWiFS, *J. Geophys. Res.*, *103*, 24,937–24,953.

O'Reilly, J. E., et al. (2000), Ocean color chlorophyll a algorithms for SeaWiFS, OC2 and OC4: Version 4, *NASA Tech. Mem.*, *2000-206892*, vol. 11.

Pegau, W. S. (2002), Inherent optical properties of the central Arctic surface waters, *J. Geophys. Res.*, *107*(C10), 8035, doi:10.1029/2000JC000382.

Pegau, W. S., et al. (1995), A comparison of methods for the measurement of the absorption coefficient in natural waters, *J. Geophys. Res.*, *100*, 13,201–13,220.

Pegau, W. S., D. Gray, and J. R. V. Zaneveld (1997), Absorption of visible and near-infrared light in water: The dependence on temperature and salinity, *Appl. Opt.*, *36*, 6035–6046.

Peterson, B. J., R. M. Holmes, J. W. McClelland, C. J. Vorosmarty, R. B. Lammers, A. L. Shiklomanov, I. A. Shiklomanov, and S. Rahmstorf (2002), Increasing river discharge to the Arctic Ocean, *Science*, *298*, 2171–2173.

Reynolds, R. A., D. Stramski, and B. G. Mitchell (2001), A chlorophyll-dependent semianalytical reflectance model derived from field measurements of absorption and backscattering coefficients within the Southern Ocean, *J. Geophys. Res.*, *106*, 7125–7138.

Risović, D. (2003), Effect of suspended particulate-size distribution on the backscattering ratio in the remote sensing of seawater, *Appl. Opt.*, *41*, 7092–7101.

Sathyendranath, S., G. Cota, V. Stuart, H. Maass, and T. Platt (2001), Remote sensing of phytoplankton pigments: A comparison of empirical and theoretical approaches, *Int. J. Remote Sens.*, *22*, 249–273.

Stramski, D., and D. A. Kiefer (1991), Light scattering by microorganisms in the open ocean, *Prog. Oceanogr.*, *28*, 343–383.

Strickland, J. D., and T. R. Parsons (1972), Pigment analysis, in *A Practical Handbook of Seawater Analysis*, pp. 185–196, Fish. Res. Board of Canada, Ottawa.

Twardowski, M., E. Boss, J. B. Macdonald, W. S. Pegau, A. H. Barnard, and J. R. Zaneveld (2001), A model for estimating bulk refractive index from the optical backscattering ratio and the implications for understanding particle composition in case I and II waters, *J. Geophys. Res.*, *106*, 14,129–14,142.

Ulloa, O., S. Sathyendranath, and T. Platt (1994), Effect of the particle-size distribution on the backscattering ratio in seawater, *Appl. Opt.*, *33*, 7070–7077.

Wang, J., and G. F. Cota (2003), Remote-sensing reflectance in the Beaufort and Chukchi Seas: Observations and models, *Appl. Opt.*, *44*, 2754–2765.

————————————

G. F. Cota, D. A. Ruble, and J. Wang, Center for Coastal Physical Oceanography, Department of Ocean, Earth, and Atmospheric Sciences, Old Dominion University, 768 W. 57nd Street, Norfolk, VA 23508, USA. (cota@ccpo.odu.edu; ruble@ccpo.odu.edu; wang@ccpo.odu.edu)